Chemical Physics Letters 522 (2012) 17–22

Contents lists available at SciVerse ScienceDirect

Chemical Physics Letters

journal homepage: www.elsevier.com/locate/cplett

Morphed intermolecular potential of OC:HCCH complex based on infrared quantum cascade laser spectroscopy

Luis A. Rivera-Rivera, Blake A. McElmurry, Zhongcheng Wang, Igor I. Leonov, Robert R. Lucchese, John W. Bevan *

Department of Chemistry, Texas A&M University, College Station, TX 77843-3255, United States

ARTICLE INFO

Article history:
Received 19 October 2011
In final form 21 November 2011
Available online 2 December 2011

ABSTRACT

Spectroscopic studies of the OC:HCCH complex are reported using a continuous supersonic slit jet spectrometer with broadband frequency mode-hop free tunable infrared quantum cascade lasers (QCL), centered at 4.4 and 4.6 μm. This Letter includes an extended analysis of the ν_3 CO stretching vibration frequency, and investigation of the $\nu_3 + \nu_9^1 - \nu_9^1$ hot band, the $\nu_3 + \nu_9^1$ and $\nu_3 + \nu_8^1$ combination bands for OC–HCCH. The ground state low frequency bend, ν_9^1, is determined at 20.48361(20) cm^{-1}. The generated rovibrational data is incorporated with previously determined information and used to generate a four-dimensional compound-model morphed potential with radial correction, giving further insight into the molecular dynamics of this complex.

1. Introduction

The OC:HCCH complex has been subject of previous experimental supersonic jet investigations using microwave [1–3] and also infrared [4–9] spectroscopies in the CO and CH fundamental frequency regions. The complex has also been the subject of additional theoretical work [10–13]. These investigations indicated that the ground state structure of the complex is quasi-linear with the atoms ordering as OC–HCCH, with $R_0 = 5.0167(3)$ Å [3]. Significant perturbations have been observed in the infrared spectra recorded in both the CO and CH stretching regions of the complex [4,6,8]. In contrast, in the OC–DCCH complex, perturbations in the CH region are not observed [9], due to the decoupling of CH vibration from the intermolecular vibrational modes. Currently, no work on experimental studies of the rovibrational energy manifold associated with the ground state intermolecular vibrations of the complex have been completed. Such information would provide accurate data that form the basis for refining modeling of the intermolecular potential energy surface in the complex. In the present Letter, hot bands and combination bands associated with the ν_3 CO stretching vibration frequency and the low frequency bend, ν_9^1, are reported for the OC–HCCH complex using a cw slit jet expansion. This newly recorded rovibrational data is used with previously recorded spectroscopic information to generate a four-dimensional (4-D) compound-model morphed potential with radial correction, which can then serve as a model with which to further characterize the structure and molecular dynamics of the dimer.

2. Experimental methods

The cw slit jet infrared quantum cascade laser (QCL) spectrometer used in the current investigations is based on a similar design to that of a previously constructed lead salt continuous slit jet semiconductor laser spectrometer but with accommodations necessary for substitution of quantum cascade lasers (QCLs) as sources [14]. The quantum cascade lasers (QCLs) employed in the current investigations were fabricated by Daylight Solutions (San Diego, California) and have mode-hop free operational ranges from 2145 to 2195 cm^{-1} (21045-MHF) and 2194 to 2300 cm^{-1} (21043-MHF), respectively. Details of the QCL spectrometer have been given elsewhere [15], thus a short description of the instrument will be given in this Letter. The laser controllers were connected via GPIB interface to the host computer and the output frequency and power of the laser head could be set by a custom LabVIEW program with integrated vi's from the manufacturer. Water cooling is supplied by a Thermo CUBE 200 Watt recirculating chiller (Solid State Systems, Pleasant Valley, NY). Tuning of the output frequency of the QCL head can be achieved by two methods. Coarse tuning of the output frequency determined by controlling a stepping motor that changes the QCL cavity length through a pivoted external cavity grating while sustaining a single cavity mode. Fine-tuning used for the spectroscopic measurements is accomplished by an applied voltage to a piezo-electric device in the range 0–100 to mechanically move the grating to cover an incremental 2.0 cm^{-1} range. The voltage applied to the PZT was generated by a NI PCI-6251

* Corresponding author. Fax: +1 979 8454719.
E-mail address: bevan@mail.chem.tamu.edu (J.W. Bevan).

0009-2614/$ - see front matter © 2011 Elsevier B.V. All rights reserved.
doi:10.1016/j.cplett.2011.11.072

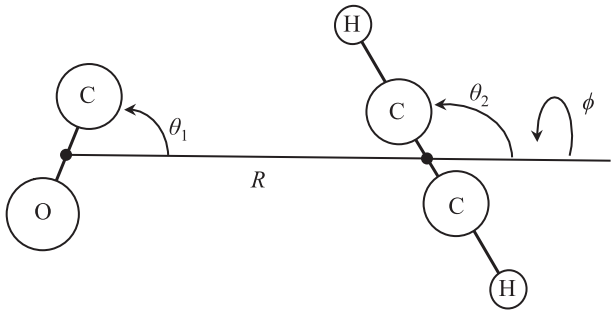

Figure 1. Geometry of OC:HCCH dimer in Jacobi coordinates.

analog output and MDT694A Piezo controller. Laser output powers in the range 80–100 mW are typical once threshold emission had been achieved. Wavelength modulation of the laser source was achieved by the application of a sinusoidal waveform with a frequency of 10 kHz to 2 MHz (M_F) and a modulation amplitude, M_A, of ±2 V DC giving up to 0.05 cm^{-1} modulation amplitude in frequency. Frequency tunability and single mode-hop free operation was characterized to have a free-running linewidth of <30 MHz. The output of the laser was first split by a CaF_2 wedge and following redirection by a reflection mirror, split again into three components using CaF_2 beam splitters. The transmitted beam from the first CaF_2 beam splitter was collected by a Wood's horn to reduce back reflections and eliminate feedback to the QCL chip. The total power used in the current experiment is estimated to be about 0.8 mW. The detectors used in the current study were LN_2 cooled InSb detectors (Graesby Infrared or Infrared Associates) and preamplifiers having a 1 MHz bandwidth. The output of these detectors were sampled by three EG&G 5302 lock-in amplifiers referenced to the modulation signal. The output of the lock-in amplifiers were digitized and stored in the computer using the LabVIEW program and DAQ interface. The absolute frequency scale of the observed spectrum was determined by a combination of passive Fabry–Perot confocal etalon (Spectra-Physics, SP5945) with a FSR of 0.00962456 cm^{-1} referenced to carbon monoxide (1 Torr, 30 cm path) and nitrous oxide (10 Torr, 10 cm path) standard transitions from the HITRAN database that were used for calibration of absolute frequencies to an accuracy of ±0.0005 cm^{-1}. The 12 cm long slit jet expansion was formed from a reservoir sample maintained at a total pressure in the range 15–30 psi consisting of typically 0.5–1% acetylene, 5% carbon monoxide mixed with 94% argon carrier and spectra recorded with single pass of the radiation source through the supersonic jet expansion. The vacuum chamber housing the slit expansion was pumped to 600 mTorr by a Leybold RA2001 Roots blower and a Leybold SV630F roughing pump.

3. Theoretical methods

3.1. Ab initio calculations of OC:HCCH

The non-relativistic *ab initio* interaction energies of the OC:HCCH complex was calculated using the MOLPRO 2009 electronic structure package [16]. In this Letter, we have calculated three *ab initio* potentials: (i) CCSD(T)/aug-cc-pVTZ, (ii) MP2/aug-cc-pVQZ, (iii) MP2/aug-cc-pVTZ. These three potentials were corrected for the basis set superposition error (BSSE) using the counterpoise (CP) correction of Boys and Bernardi [17]. All of these three *ab initio* potentials were calculated on a 4-D grid (R, θ_1, θ_2, ϕ) (Figure 1) of 6096 points. The variable R, takes the values of 4.25, 4.50, 4.75, 5.00, 5.25, 5.50, 5.75, 6.00, 6.50, 7.00, 7.50, and 8.00 Å. The angle θ_1 takes the values of 10.0°, 45.0°, 80.0°, 100.0°, 135.0°, and 170.0° while the angle θ_2 the values of 10.0°, 45.0°, 80.0°, and 90.0°. Additional values of θ_2 = 100.0°, 135.0°, and 170.0° were obtained by symmetry. Lastly, the dihedral angle ϕ was chosen with values of 10.0°, 45.0°, 80.0°, 100.0°, 135.0°, and 170.0°. The additional values of ϕ = 190.0°, 225.0°, 260.0°, 280.0°, 315.0°, and 350.0° were obtained by symmetry. The 4-D grid was supplemented with additional points at all values of R and with ϕ = 0.0°, θ_1 = 0.0°, 180.0°, and θ_2 = 0.0°. The additional value of θ_2 = 180.0° was obtained by symmetry. In all calculations, the bond lengths of the monomers component were fixed at 1.128323 Å for C–O [18], 1.20286 Å for C–C [19], and 1.06166 Å for C–H [19].

3.2. Fitting of the ab initio potentials

In order to have a global representation of the interaction potential, the calculated *ab initio* points, at each value of R_i were fitted to the spherical expansion [20,21]:

$$V(R_i,\theta_1,\theta_2,\phi) = \sum_{\Lambda} v_{\Lambda,i} A_{\Lambda}(\theta_1,\theta_2,\phi) \quad (1)$$

In Eq. (1), Λ is a collective symbol for the quantum numbers (L_1,L_2,L), $v_{\Lambda,i}$ are the expansion coefficients [22,23], and $A_{\Lambda}(\theta_1,\theta_2,\phi)$ have been given before [23]. The expansion coefficients were evaluated using standard least-squares procedure [23].

The radial potential is obtain by interpolating the angular potential on the grid of R_i points, at fixed angular coordinates, using a 1-D radial reproducing kernel of the form:

$$V(R,\theta_1,\theta_2,\phi) = (V_{\min})\left[\exp\left(\sum_i \alpha_i,(\theta_1,\theta_2,\phi) q_1^{2,6}(R_i,R)\right) - 1\right] \quad (2)$$

In Eq. (2), $V_{\min}$ was chosen to be 600.0 cm^{-1} and the function $q_1{}^{2,6}$ is a 1-D radial reproducing kernel [24].

3.3. Rovibrational energy calculations

The rovibrational Hamiltonian used in this Letter is the same as the one used before for two interacting linear rotors [23], where the vibrational problem is reduced to a 4-D problem. Thus, the rovibrational energy levels can be calculated using the pseudo-spectral approach discussed previously [23,25,26]. The convergence of the rovibrational energy calculations depends on the selection of the following parameters: R_{start} = 4.250 Å (the first point of the R radial grid), R_{end} = 8.000 Å (the last point of the R

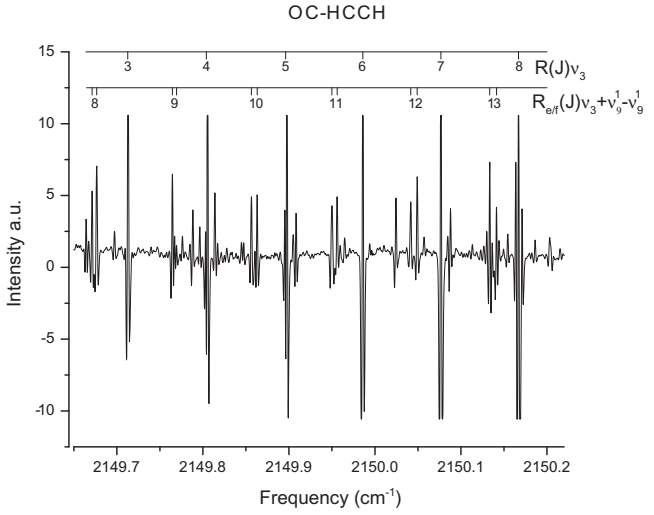

Figure 2. Segment of the supersonic jet spectrum of $^{16}O^{12}C$–$H^{12}C^{12}CH$ recorded using a cw slit jet QCL spectrometer showing the ν_3, CO stretching vibration, and $\nu_3 + \nu_9^1 - \nu_9^1$ hot band.

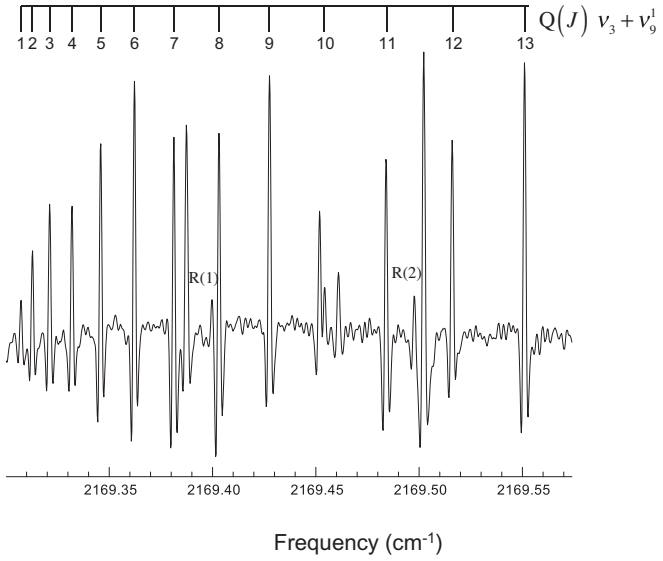

Figure 3. Segment of the supersonic jet spectrum of $^{16}O^{12}C$–$H^{12}C^{12}CH$ recorded using a cw slit jet QCL spectrometer showing the $\nu_3 + \nu_9^1$ combination band.

radial grid), $N_R = 46$ (the number of grid points in the R radial direction), $N_{\theta_1} = N_{\theta_2} = 24$ (the number of θ_1 and θ_2 points used in the grid), and $N_\phi = 40$ (the number of ϕ points used in the grid). The number of radial spectral basis functions is $N_F = 42$. All of the summations over spectral states are truncated so that $j_{max_1} = 18$ and $j_{max_2} = 18$, and include all possible values of m_1 and m_2. The tolerance (τ_L) used to determine the convergence of the eigenvalues in the Lanczos procedure [27] was 10^{-12} atomic units. In the kinetic energy expression the rotational constant of the free monomers were used: 1.176608 cm^{-1} for HCCH [28], 0.847887 cm^{-1} for DCCD [28], 0.9915273 cm^{-1} for DCCH [28], and 1.92252905 cm^{-1} for CO [29].

3.4. Compound-model morphing method with radial correction

In the compound-model morphing method with radial correction (CMM-RC), the potential is generated as:

$$V_{CMM-RC}(R) = C_1\left[V_{MP2/QZ}(R')\right] + C_2\{\left[V_{CCSD(T)/TZ}(R')\right] - \left[V_{MP2/TZ}(R')\right]\},$$
$$R' = C_3(R - R_f) + (1.0 + C_4)R_f \quad (3)$$

where the C_α are the unitless morphing parameters. The reference or unmorphed potential, $V^{(0)}_{CMM-RC}$, is obtained by initially choosing $C_1 = 1.0$, $C_2 = 1.0$, $C_3 = 1.0$, and $C_4 = 0.0$. The morphing parameters C_α are determined by using a regularized nonlinear least-squares optimization [30], that minimized:

$$F(C_\alpha, \gamma) = \sum_{k=1}^{M}\left\{\frac{O_k^{expt} - O_k^{calc}(C_\alpha)}{\sigma_k}\right\}^2 + \gamma^2\sum_\alpha\left(C_\alpha - C_\alpha^{(0)}\right)^2 \quad (4)$$

In Eq. (4), the $C_\alpha^{(0)}$ are the values of the morphing parameters for the reference or unmorphed potential and γ is the regularized parameter, and was chosen to be 10.0. In Eq. (3), the parameter C_1 is the scaling parameter for the interaction energy of the dimer at the MP2/aug-cc-pVQZ level of theory including the CP correction for the BSSE. The second term in Eq. (3) corrects for the correlation energy at the CCSD(T) level of theory. Lastly, the radial correction is included with the parameters $C_3$and C_4, and the value of R_f was chosen to be 5.00 Å. The quality of the fit of the experimental data is characterized by the root mean square (RMS) deviation of the experimental data:

$$G(\gamma) = \left[\frac{1}{M}\sum_{K=1}^{M}\left\{\frac{O_k^{expt} - O_k^{calc}(C_\alpha)}{\sigma_k}\right\}^2\right]^{1/2} \quad (5)$$

Table 2
Experimental data used in the CMM-RC fits for OC:HCCH.

Observable[a]	Isotopomer	$V^{(0)}_{CMM-RC}$	$V^{(3)}_{CMM-RC}$	Exp.	σ_k
B (GS)/10^{-2} cm^{-1}	$^{16}O^{12}C$–$H^{12}C^{12}CH$	4.667	4.665	4.661[b]	0.002
D_J (GS)/10^{-8} cm^{-1}	$^{16}O^{12}C$–$H^{12}C^{12}CH$	16.0	17.2	17.6[b]	0.2
B (GS)/10^{-2} cm^{-1}	$^{16}O^{12}C$–$D^{12}C^{12}CD$	4.435	4.432	4.435[b]	0.002
D_J (GS)/10^{-8} cm^{-1}	$^{16}O^{12}C$–$D^{12}C^{12}CD$	13.7	14.8	14.5[b]	0.2
B (GS)/10^{-2} cm^{-1}	$^{16}O^{12}C$–$D^{12}C^{12}CH$	4.651	4.648	4.653[b]	0.002
D_J (GS)/10^{-8} cm^{-1}	$^{16}O^{12}C$–$D^{12}C^{12}CH$	15.6	16.8	16.6[b]	0.2
B (GS)/10^{-2} cm^{-1}	$^{16}O^{12}C$–$H^{12}C^{12}CD$	4.448	4.445	4.440[c]	0.002
ν_9^1/cm^{-1}	$^{16}O^{12}C$–$H^{12}C^{12}CH$	20.54	20.48	20.48[d]	0.01
B (ν_9^1)/10^{-2} cm^{-1}	$^{16}O^{12}C$–$H^{12}C^{12}CH$	4.77	4.77	4.80[d]	0.02
D_J (ν_9^1)/10^{-8} cm^{-1}	$^{16}O^{12}C$–$H^{12}C^{12}CH$	20.0	21.4	28.0[d]	3.0
G		4.1	1.8		

[a] GS = ground state.
[b] From [1].
[c] From [2].
[d] This Letter.

4. Results and discussion

A short frequency segment in the range 2149.65–2150.22 $cm^{-1}$of the recorded spectrum for OC–HCCH is presented in Figure 2. The $R(3)$ to $R(8)$ transitions of the ν_3 CO stretching vibration for OC–HCCH are illustrated in Figure 2, as well as the $R_{e,f}(8) - R_{e,f}(13)$ transitions of the $\nu_3 + \nu_9{}^1 - \nu_9{}^1$ hot band. A total of 76 transitions of the former were recorded from $P(40)$ to $R(36)$ while transitions from $P(30)$ to $R(17)$ were recorded for the latter. In addition, the $\nu_3 + \nu_9{}^1$ combination band of the low frequency bend of the complex has also been observed and a short frequency segment of that spectrum showing the $Q(1)$ to $Q(13)$ transitions is given in Figure 3. In this case, $Q(1)$ to $Q(28)$ were recorded and measured together with $R(J)$ and $P(J)$ transitions from $R(2)$ to $R(22)$ and $P(3)$ to $P(23)$. The measured transition frequencies for

Table 1
Rovibrational data measured using the QCL spectrometer.

Observable	GS OC–HCCH	ν_9^1 OC–HCCH	ν_3 OC–HCCH	$\nu_3 + \nu_9^1$ OC–HCCH	$\nu_3 + \nu_8^1$ OC–HCCH
ν_0/cm^{-1}		20.48361(20)	2149.34326(15)	2169.30453(16)	2219.77212(36)
B/cm^{-1}	0.0466092(25)	0.0479734(30)	0.0464494(26)	0.0478623(30)	0.0465011(33)
D_J/cm^{-1}	$1.715(15) \times 10^{-7}$	$2.801(30) \times 10^{-7}$	$1.728(16) \times 10^{-7}$	$2.909(32) \times 10^{-7}$	$1.1(1) \times 10^{-7}$
q/cm^{-1}		$2.3257(71) \times 10^{-4}$		$2.3937(62) \times 10^{-4}$	

$\nu_3 + \nu_9^1 - \nu_9^1 = 2148.82092(16)$ cm^{-1}

Table 3
Optimized values for the morphing parameters for OC:HCCH.

α	$C_\alpha^{(0)}$	$C_\alpha^{(3)}$	σ
1	1.0	0.99276	0.00091
2	1.0	(1.0)	Constrained
3	1.0	0.96470	0.00370
4	0.0	−0.00052	0.00012

these bands were fitted and used to provide the molecular constants given in Table 1. Our measured value of ν_3 of 2149.34326(15) cm^{-1} agrees very well with previously determined values of 2149.3444(13) cm^{-1} [7] and 2149.3435(2) cm^{-1} [8]. The rotational intensity distributions are consistent with an effective temperature distribution of 12(2) K. The newly generated data for the low frequency bend, $\nu_9{}^1$ was obtained by combination frequency differences together with previous microwave data [1,2] that was then used to morphed the intermolecular potential energy surface of OC:HCCH, as given in Table 2. The value of morphing parameters, C_α, are also provided in Table 3. As shown in Table 2, the unmorphed potential is in good agreement with the experimental observables, as indicated by the determined value of $G = 4.1$. The final morphed potential has small but significant improvement in reproducing the experimental data, as the final value has decreased to $G = 1.8$. The relatively small change in the potential after morphing can be seen in the small change in the morphing parameter from the reference value, as shown in Table 3. An attempt to correct for the BSSE was made by including in Eq. (3) the term $[(V^{CP}_{CCSD(T)/TZ}) - (V^{NOCP}_{CCSD(T)/TZ})$, but the correction was not significant in this case.

Two-dimensional slices of the morphed potential energy surface of OC:HCCH are shown in Figure 4. This surface is characterized by two identical linear global minima OC–HCCH, due to the HCCH symmetry, having $R_e = 5.018(2)$ Å and $D_e = 360(4)$ cm^{-1}. The R_e value can be compared to the determined value from the microwave analysis of 5.0011 Å [2] and 4.9672 Å [3]. In addition, previous theoretical work gave $R_e = 5.014$ Å and $D_e = 211$ cm^{-1} [31]. Also the potential surface has two identical secondary linear minima CO–HCCH, which have not been observed experimentally, with $R_e = 4.671(4)$ Å and $D_e = 232(10)$ cm^{-1}. Previous theoretical work gave $R_e = 4.688$ Å and $D_e = 167$ cm^{-1} [31]. The energy difference between the two minima is 128(10) cm^{-1}. Previous predictions gave a value of 400 cm^{-1} [4], 258 cm^{-1} [12], 44 cm^{-1} [31], and 26 cm^{-1} [11]. The predicted ground state structure of the $^{16}O^{12}C$–$H^{12}C^{12}CH$ complex from the morphed potential is: $\bar{\theta}_i = \cos^{-1}(\langle\cos^2\theta_i\rangle^{1/2})$ for $i = 1$ and 2, $\bar{\theta}_1 = 18.8°$, $\bar{\theta}_2 = 163.2°$, and $R_0 = 5.0167$ Å. These structural parameters compare with the values: $\bar{\theta}_1 = 11.30°$, $\bar{\theta}_2 = 166.38°$, and $R_0 = 5.0167(3)$ Å, determined from the microwave analysis [3]. Another microwave analysis gave the value of $\bar{\theta}_2 \approx 160°$ and $R_0 = 5.018(6)$ Å [2]. Moreover, the morphed potential prediction, for $^{16}O^{12}C$–$H^{12}C^{12}CH$, is consistent with a D_0 value of 232(4) cm^{-1}, $\nu_5 = 53.5(4)$ cm^{-1} (the hydrogen bond stretching frequency), and $\nu_8{}^1 = 73.7(2)$ cm^{-1} (the high frequency bend of the complex). These predictions of the intermolecular

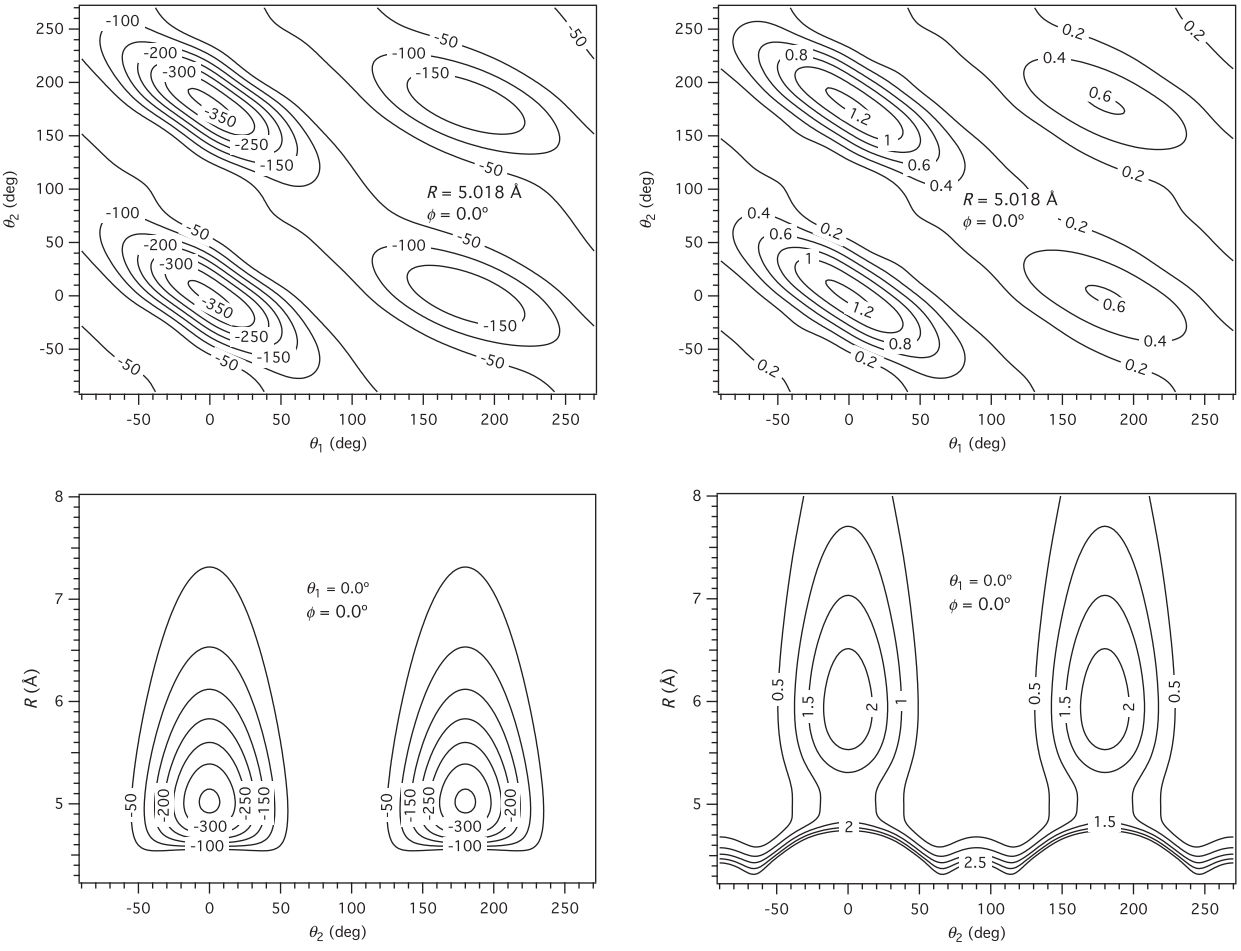

Figure 4. Two-dimensional slices of the interaction morphed potential ($V^{(3)}_{CMM-RC}$), of $^{16}O^{12}C$:$H^{12}C^{12}CH$ are shown in the left panels. The corresponding estimated errors relative to the potential at infinite separation are shown in the right panels. The coordinates used are the Jacobi coordinates defined in Figure 1. All contours are in cm^{-1}.

Table 4
Comparison of the vibrational frequencies for $^{16}O^{12}C$–$H^{12}C^{12}CH$.

Reference	ν_5 (cm^{-1})	ν_8^1 (cm^{-1})	ν_9^1 (cm^{-1})
[11]	62	57	12
[12]	70	95	40
[13]	64	89	28
[31]	69.9	96.3	38.9
This Letter	53.5	73.7	20.48

stretching fundamentals to be $\nu_5 = 53.5(4)\,cm^{-1}$ and $\nu_8^1 = 73.7(2)\,cm^{-1}$ are consistent with substantial depopulation in the jet expansion of excited states that prevented experimental observation of their respective hot bands $\nu_3 + \nu_5 - \nu_5$ and $\nu_3 + \nu_8^1 - \nu_8^1$. Our prediction for ν_5 can be compared with the value of 46.4 cm^{-1} evaluated from the microwave analysis [2]. In addition, the D_0 value for $^{12}C^{16}O$–$H^{12}C^{12}CH$ isomer is predicted to be at $146(10)\,cm^{-1}$. The isomerization energy for the $^{16}O^{12}C$–$H^{12}C^{12}CH$ isomer relative to the $^{12}C^{16}O$–$H^{12}C^{12}CH$ isomer is then predicted to be $86(10)\,cm^{-1}$ and as a consequence, we were also unable to experimentally identify rovibrational transitions associated with this less stable isomer experimentally. Previous results suggested the possibility of coexistence of these two isomers at wide temperature intervals [32]. The predicted ground state structure for the $^{12}C^{16}O$–$H^{12}C^{12}CH$ isomer from the morphed potential is: $\bar{\theta}_i = \cos^{-1}(\langle\cos^2\theta_i\rangle^{1/2})$ for $i = 1$ and 2, $\bar{\theta}_1 = 205.4°$, $\bar{\theta}_2 = 160.8°$, and $R_0 = 4.676$ Å.

In Table 4, the previous calculated harmonic vibrational frequencies for $^{16}O^{12}C$–$H^{12}C^{12}CH$are compared with the corresponding values predicted from the morphed potential. The generated harmonic frequencies range from being either larger or too small relative to the corresponding predictions based on the current morphed potential. Our predicted D_e and D_0 values are respectively 360(4) and 232(4) cm^{-1} for the $^{16}O^{12}C$–$H^{12}C^{12}CH$ complex and can be compared with previous predictions of $D_e = 318\,cm^{-1}$ and $D_0 = 218\,cm^{-1}$ [11]. In addition, the predicted D_e and D_0 values of 232(10) and $146(10)\,cm^{-1}$, respectively for the $^{12}C^{16}O$–$H^{12}C^{12}CH$ complex, are in contrast to the previous prediction of $D_e = 344\,cm^{-1}$ and $D_0 = 250\,cm^{-1}$ [11]. In addition, from the microwave analysis, the D_e for $^{16}O^{12}C$–$H^{12}C^{12}CH$ were estimated to be 299 cm^{-1} [2] and 295.4 cm^{-1} [3].

As shown in Table 2, the rotational and distortion constants of the ν_9^1 bending frequency of $^{16}O^{12}C$–$H^{12}C^{12}CH$ complex are not well reproduced. This discrepancy can be attributed to Coriolis perturbations centered at certain J levels. Moreover, a preliminary analysis of the spectrum using combination differences of the $\nu_3 + \nu_8^1$ band indicates significant perturbations only in the upper state. From this data, the ν_8^1 in the upper state is determined to be at approximately $70.4289(4)\,cm^{-1}$. This value can be compared to the ν_8^1 predicted in the ground state to be $73.7(2)\,cm^{-1}$ from the morphed potential. The observed shift can be expected to result from a contribution from vibrational coupling and possible perturbation with a dark state. In the $\nu_3 + \nu_8^1$ e state there is evidence for Coriolis perturbations centered at $J' = 7$ and $J' = 18$. In addition, there is an extensive additional Coriolis perturbation in the $\nu_3 + \nu_8^1$ f state centered at $J' = 10$. These analyses are confirmed by no evidence for perturbation in the lower state as determined by combination frequency differences.

Even though the potential of the OC–HCCH complex has two symmetric wells associate with a rotation of the HCCH component, no significant tunneling splitting is observed. According to our calculations the tunneling splitting in the ground state is very small ($\sim 6.7 \times 10^{-6}\,cm^{-1}$), practically zero within numerical error. As shown in Figure 4, the large and wide barrier of $\sim 360(4)\,cm^{-1}$ implies a very localized wave function where the tunneling probability is nearly zero. In addition, since the inversion symmetry of acetylene monomer is broken on complexation, the normal mode picture is not completely valid [9]. Therefore, tunneling splitting also may not be observed due to the dynamic nature of the complex.

5. Conclusions

A spectroscopic investigation of intermolecular hot bands and combination bands in the ν_3 (CO stretching region) using a cw slit jet expansion in a quantum cascade laser spectrometer has extended analysis of the structure and dynamics of the OC–HCCH complex. From this experimental data, the ground state low frequency bend, ν_9^1, is determined to be at $20.48361(20)\,cm^{-1}$ while a generated intermolecular morphed potential can be used to predict the intermolecular stretching fundamental to be $\nu_5 = 53.5(4) cm^{-1}$ and the high frequency bend of the complex to be $\nu_8^1 = 73.7(2)\,cm^{-1}$. A precise experimental determination of the D_0 and D_e values for OC–HCCH and CO–HCCH are not available but the current morphed potential predicts values of 360(4) and $232(4)\,cm^{-1}$ for OC–HCCH, and 232(10) and $146(10)\,cm^{-1}$ for CO–HCCH, respectively. The isomerization energy OC–HCCH/CO–HCCH using the available morphed potential is predicted to be $86(10)\,cm^{-1}$ and explains our failure to observe this isomer with current instrumental capabilities. Our present analyses of $\nu_3 + \nu_9^1 - \nu_9^1$ low frequency bending vibrational hot band in the OC stretching vibration of the complex indicates extensive Coriolis interaction in the excited states of this vibration that will have to be considered before a more accurate complete potential can be generated for this complex.

Acknowledgements

We wish to thank the National Science Foundation (NSF 0911695, CHE-0613202 and CHE-0541587) as well as the LST/ST TAMU for supporting this research. In addition, we express special thanks to the Robert A Welch Foundation (Grant A747) for financial support in the form of a post-doctoral fellowship for Blake A. McElmurry. We also thank the Laboratory for Molecular Simulation, the Supercomputing Facility, and the Brazos HPC cluster at Texas A&M University for providing support, and computer time.

References

[1] A.C. Legon, A.L. Wallwork, J.W. Bevan, Z. Wang, Chem. Phys. Lett. 180 (1991) 57.
[2] M.A. Roehrig, S.G. Kukolich, Chem. Phys. Lett. 188 (1992) 232.
[3] T.C. Germann, S.L. Tschopp, H.S. Gutowsky, J. Chem. Phys. 97 (1992) 1619.
[4] M.D. Marshall, D.G. Prichard, J.S. Muenter, J. Chem. Phys. 90 (1989) 6049.
[5] M.D. Marshall, J. Kim, T.A. Hu, L.H. Sun, J.S. Muenter, J. Chem. Phys. 94 (1991) 6334.
[6] R.D. Beck, A.G. Maki, S.H. Tseng, R.O. Watts, J. Mol. Spectrosc. 158 (1993) 306.
[7] Y. Kawashima, K. Nishizawa, Chem. Phys. Lett. 253 (1996) 77.
[8] J.A. Anstey, M.D. Brookes, A.R.W. McKellar, J. Mol. Spectrosc. 194 (1999) 281.
[9] I. Hunig, L. Oudejans, R.E. Miller, J. Mol. Spectrosc. 204 (2000) 148.
[10] S.A.C. McDowell, A.D. Buckingham, Chem. Phys. Lett. 182 (1991) 551.
[11] C.A. Parish, J.D. Augspurger, C.E. Dykstra, J. Phys. Chem. 96 (1992) 2069.
[12] L. Adamowicz, Chem. Phys. Lett. 192 (1992) 199.
[13] W.B. De Almeida, J.S. Craw, Chem. Phys. 169 (1993) 185.
[14] A.L. McIntosh, Z. Wang, R.R. Lucchese, J.W. Bevan, Infrared Phys. Technol. 45 (2004) 301.
[15] B.A. McElmurry, L.A. Rivera-Rivera, K.W. Scott, Z. Wang, I.I. Leonov, A.C. Legon, R.R. Lucchese, J.W. Bevan, J. Phys. Chem. A, submitted for publication.
[16] H.-J. Werner, P.J. Knowles, R. Lindh, F.R. Manby, M. Schütz, P. Celani, T. Korona, A. Mitrushenkov, G. Rauhut, T.B. Adler, R.D. Amos, A. Bernhardsson, A. Berning, D.L. Cooper, M.J.O. Deegan, A.J. Dobbyn, F. Eckert, E. Goll, C. Hampel, G. Hetzer, T. Hrenar, G. Knizia, C. Köppl, Y. Liu, A.W. Lloyd, R.A. Mata, A.J. May, S.J. McNicholas, W. Meyer, M.E. Mura, A. Nicklass, P. Palmieri, K. Pflüger, R. Pitzer, M. Reiher, U. Schumann, H. Stoll, A.J. Stone, R. Tarroni, T. Thorsteinsson, M. Wang, A. Wolf, MOLPRO, version 2009.1, a package of ab initio programs, Cardiff, UK, 2009.
[17] S.F. Boys, F. Bernardi, Mol. Phys. 19 (1970) 553.
[18] K.P. Huber, G. Herzberg, Molecular Spectra and Molecular Structure iv; Constants of Diatomic Molecules, van Nostrand Reinhold, New York, 1979.

[19] J. Lievin, J. Demaison, M. Herman, A. Fayt, C. Puzzarini, J. Chem. Phys. 134 (2011) 064119.
[20] A. van der Avoird, P. Wormer, F. Mulder, R. Berns, Top. Curr. Chem. 93 (1980) 1.
[21] A. van der Avoird, P.E.S. Wormer, R. Moszynski, Chem. Rev. 94 (1994) 1931.
[22] S. Green, J. Chem. Phys. 62 (1975) 2271.
[23] J. Castillo-Chara, J.W. Bevan, R.R. Lucchese, Comput. Phys. Commun. 145 (2002) 48.
[24] T.S. Ho, H. Rabitz, J. Chem. Phys. 104 (1996) 2584.
[25] C. Leforestier, L.B. Braly, K. Liu, M.J. Elrod, R.J. Saykally, J. Chem. Phys. 106 (1997) 8527.
[26] G. Brocks, A. van der Avoird, B.T. Sutcliffe, J. Tennyson, Mol. Phys. 50 (1983) 1025.
[27] J.K. Cullum, R.A. Willoughby, Lanczos Algorithms for Large Symmetric Eigenvalue Computations, Birkhäuser, Boston, 1985.
[28] A. Baldacci, S. Ghersetti, S.C. Hurlock, K. Narahari Rao, J. Mol. Spectrosc. 59 (1976) 116.
[29] P.D. Soper, A.C. Legon, W.H. Flygare, J. Chem. Phys. 74 (1981) 2138.
[30] J. Castillo-Chara, R.R. Lucchese, J.W. Bevan, J. Chem. Phys. 115 (2001) 899.
[31] B. Wang, Y. Gu, F. Kong, J. Phys. Chem. A 103 (1999) 7395.
[32] Z. Slanina, L. Adamowicz, Z. Phys. D 26 (1993) 338.